# AN EXPERIMENTAL INVESTIGATION OF A RECTANGULAR JET IMPINGING ON A FLAT SURFACE OBLIQUELY

**Hayri ACAR [*] and Veysel ATLI [**]**

**[*] Department of Aeronautical Engineering, Istanbul Technical University**
**80626 Maslak, Istanbul-Turkey**
**[**] Civil Aviation School, Erciyes University, 38039 Kayseri-Turkey**

## Abstract

*Jet impingement has many applications in aeronautics and industrial aerodynamics. The effect of the impingement angle on the jet impingement flow is studied for the Reynolds number of $1.05x10^5$. Impingement angle is taken as $0^0$, $5^0$, $10^0$, $15^0$ and $20^0$. Nondimensiomalised impingement distance is H/w = 3.08. The mean velocity and turbulence intensity profiles are measured by using a constant-temperature hot-wire anemometer. Surface pressure distributions along the impingement surface were measured for comparison with hot-wire resukts. Surface oil-film technique and smoke visualization method was used to visualize the flow pattern.*

## 1 Introduction

Jet flow is one of the most important topics in aerodynamics having many practical application. Although the impingement of a single and multiple jets on surfaces is a topic of much interest, for the oblique and normal impingement of a rectangular jet onto a plane surface, the documentation is not extensive

Jet impingement has many applications in aeronautics and industrial aerodynamics like affecting spraying, cooling, heating, drying, leaching of solids, air cushion, coating thickness control. This kind of flow also occurs under V/STOL aircraft when operating near or on the ground. The ability to optimize design of efficient VTOL aircraft equipped with powered lift-jet systems and to predict their performance requires a good understanding of this complicated flow field.

Marsters [1] and Quinn [2] showed that turbulent jet flows from rectangular nozzles exhibit "saddle-backed" velocity profiles in the spanwise direction that are related to the upstream shaping of the nozzles with large aspect ratio, say, larger than 5. In this study the aspect ratio (h/w) is chosen as 2 for this reason.

Trentacoste and Sforza [3] and Quinn [4]suggested that in three-dimensional jets from rectangular and elliptical orifices, the axial velocity decays at the same rate as that of a circular jet far downstream of the orifice, indicating to a "loss of memory" of their initial conditions.

Krothapalli et al [5] indicated that the present studies are still not complete enough to enable detailed understanding of the complex flow development of the jet issuing from a rectangular nozzle of moderate aspect ratio. All the implications of the results obtained are not yet fully understood. Further detailed investigations are clearly needed to clarify the importance of the flow at the nozzle exit and the flow structure close to it. In this study impingement distance is chosen as H/w = 3.08 which is close to the jet exit.

Page et al [6] analyzed the flowfield that develops when a radial jet reattaches to a plate. They indicated that the pressure coefficient of the flow immediately below the radial jet nozzle, the flow reattachment angle, and the flow reattachment radius are shown to be dependent on the nozzle exit shape, flow direction from the nozzle exit, nozzle to plate distance, and character of the exit flow as laminar or turbulent.

This hybrid structure, consisting of a free, deflecting flow and wall boundary layer with a free upper boundary, is ideal to test the universality of turbulence models together with predicting numerical methods, provided accurate experimental results exist [7].

Landreth and Adrian [8] measured the instantaneous velocity fields of the impinging jet flow, by using particle image velocimetry, for the first time and indicated that along the centerline, the jet acts much like a stagnation point field, forming a radial wall jet.

Özdemir and Whitelaw [9] studied the aerodynamic and thermal aspect of the wall jet flow, formed after angled impingement of an axisymmetric jet. The boundary layer formed when a round turbulent jet impinges at right angle on a flat plate spreads radially so that the radial velocities decrease slowly as the boundary layer thickness increases. The radial flow field formed after angled impingement was found to depend on the angle of impingement. Mean flow characteristics of the radial wall flow such as velocity decay and growth rate exhibit strong azimuthal dependence for all values of impingement angle, $\theta$.

The objective of this study is to investigate experimentally the rectangular jet flow that impinges to a flat plate normally and obliquelly. The effect of the impingement angle on the jet impingement flow is studied for the Reynolds number of $1.05 \times 10^5$. Impingement angle is taken as $0^0$, $5^0$, $10^0$, $15^0$ and $20^0$. Nondimensiomalised impingement distance is H/w = 3.08.

The mean velocity and turbulence intensity profiles are measured by using a constant-temperature hot-wire anemometer. In order to correlate the surface pressure distribution with hot-wire velocity results, surface pressures, relative to the pressure at settling chamber are measured by using a micromanometer. The surface oil-film technique is used to visualize the impingement surface flow pattern and smoke method is used to visualize the flow pattern of the free jet and jet impingement to a flat surface.

## 2 Instrumentation and Experimental Techniques

The open-loop, blow-down-type air supply system (ITU Aerodynamic Laboratory) with a rectangular nozzle of 100mmx50mm exit was used to provide the airflow. The nozzle has a contraction ratio of 10.5. The wall shape of the nozzle based on a third-degree polynomial. A rectangular face plate of 520mmx470mm outer dimensions is fitted at the exit of the nozzle. The aspect ratio of the nozzle defined as the ratio of exit width to exit height is w/h = 2.

The jet exit velocity, $U_0$, was founded from the difference between the static pressure at the nozzle exit and the total pressure at the settling chamber by using a micromanometer connected to a PC. The longitudinal turbulence intensity $\sqrt{\overline{u}^2}/U$ at the nozzle exit was about 1% for the exit velocity of 30 m/s. Reynolds number based on the nozzle exit width was $1.04 \times 10^5$.

For the experiments of the jet impingement, jet impinged against a flat rectangular glass plate of 490 x 980 mm. The velocity field were measured by using hot-wire anemometer and surface pressure measurements. The general arrangement of the jet and impingement surface is shown in Figure 1. Cylindrical coordinate system originates at the intersection point of the jet centerline with the impingement surface. N is normal distance above the impingement surface. $\phi$ is the azimuthal angle in ground plane where $\phi = 0^0$ is in direction of the lateral coordinate (y-axis) and $\phi = 90^0$ is in direction of the spanwise coordinate (z-axis) of the free jet. $\phi = 180^0$ line is forward, $\phi = 0^0$ line is backward, $\phi = 90^0$ and $-90^0$ lines are side directions according to the nozzle exit.

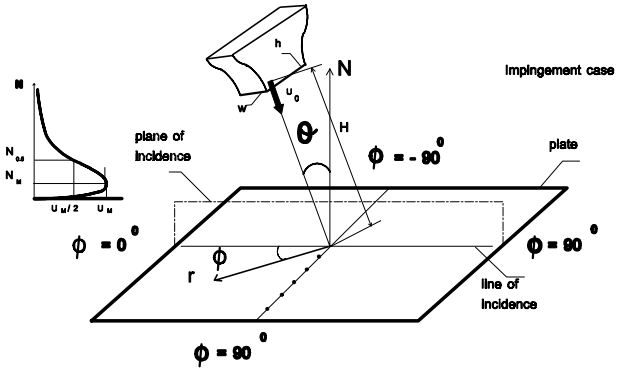


**Figure 1 General arrangement of the jet and surface.**

H is the distance from nozzle exit to the surface. θ is the angle between the jet centerline and the surface normal axis N. Plane of incidence and line of incidence are shown in Figure 1.

Smoke visualization method was used to visualize the flow pattern of jet coming from the nozzle to the impingement surface.

Surface oil-film technique was used to visualize the surface streamline after the jet impinged to the plate. Oil contains a proper mixture of gasoline, carbon dust, and conventional motor oil. The view of the skin-friction lines was recorded by a video camera.

Surface pressure distributions along the impingement surface were measured, by using pressure taps of 1 mm inner diameter drilled on the surface. ϕ is taken as $15^0$ between the pressure measurement lines and there are 13 measurement lines between $\phi = 0^0$ and $\phi = 180^0$ lines. Surface pressure distribution were measured within a half-circle of 190 mm radius.

In this study, for the hot-wire measurements a constant temperature hot-wire anemometer (CTA) system of DISA components were used. For the measurement of velocity and turbulence intensity standard type platinum-plated tungsten hot-wire probes DISA 55P01 and 55P11 were used.

A computer software named as "acqWIRE-DANTEC" was used to control the traversing system and to collect and evaluate the hot-wire data. While the measurements, number of samples: 2048, sampling interval:4096 msec, sampling frequency: 0.5 kHz were taken. The jet exit velocity was constantly monitored during acquisition. The probe traverses and data acquisition were done by automated computer control.

The uncertainty in the mean velocity and rms components of the effective velocity have the same percent error as the instantaneous velocity and estimated as less than ±1.59 %.

The hot-wire was supported in the facility by a microcomputer-controlled traversing mechanism capable of a linear motion along three axis. The sensing probe could be positioned to within 0.1 mm in the streamwise and lateral direction and to within 0.3 mm in the spanwise direction. The accuracy of the precision motion in all three directions was within ± 0.016 mm

## 3 Results and Discussion

### 3.1 The Impingement of a Rectangular Jet on a Flat Surface

For the values of H/w = 3.08, $Re_w = 1.04x10^5$, $\theta = 0^0$, flow visualization photographs are given in Figure 2 which show that, when a single jet impinges normally to a flat plate, there is three distinct regions named as a free jet region, an impingement region and a wall jet region. There is stagnation point at the intersection point of the jet centerline with the surface. Surface streak lines show an elliptical growth although nozzle has a rectangular exit like in the results of the studies [4,9]. With increasing distance from the stagnation point, the distance between the streaks increases. These results are similar with the study of Özdemir and Whitelaw [9]. Near the stagnation point, flow carries the oil at the surface due to frictional forces and this region is white in the figure between r/w = 0 and r/w ≅ 2 for $\phi = 0^0$ and r/w ≅ 2.4 for $\phi = 90^0$. After these r/w stations oil begins to accumulate which is seen gray in the figure.

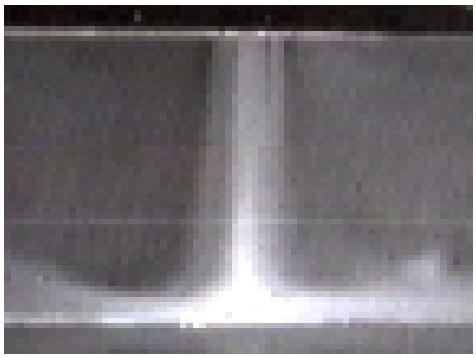

$\phi = 180^0$ impingement surface $\phi = 0^0$

$\phi = -90^0$

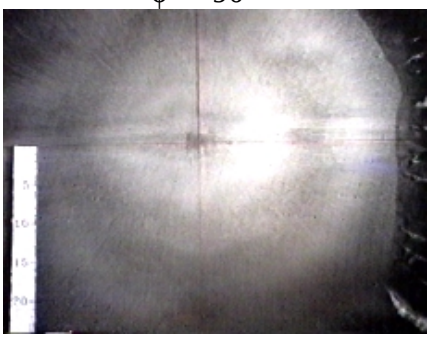

$\phi = 90^0$

**Figure 2. Smoke flow visualization photograph and surface flow pattern photograph taken by oil-film technique.**

In order to see the characteristics of the jet that impinges normally to a flat surface, the velocity and turbulence intensity profiles along $\phi = 0^0$ and $\phi = 90^0$ at different r/w stations are given in Figures 3 and 4. For the H/w = 3.08 case, jet impinges to the surface at the r/w station which is before the potential core region vanishes. Velocity profile along $\phi = 90^0$ line is wider than that of $\phi = 0^0$ line because of the rectangular shape of the nozzle exit. Near the impingement surface, velocity distribution begins to show "saddle-back" shape, which has two maximum points along $\phi = 0^0$ line and reduce values at the centerline.

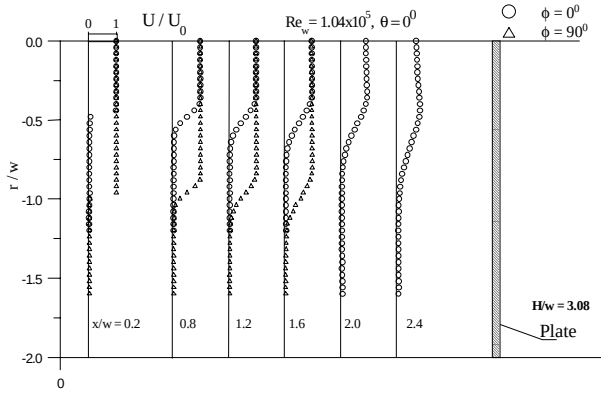


**Figure 3. The velocity distributions at different x/w stations before the impingement of the jet flow for H/w=3.08.**

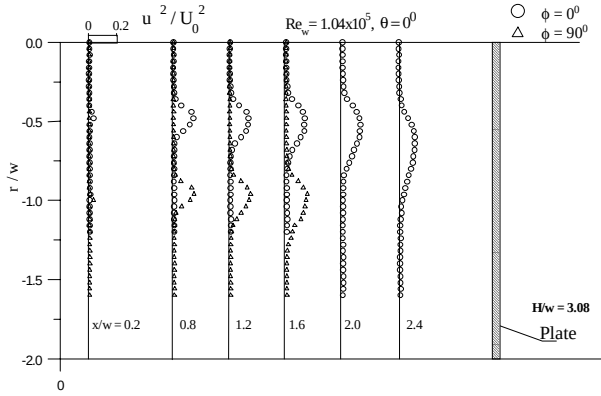


**Figure 4. The turbulence intensity distributions at different x/w stations before the impingement of the jet flow for H/w=3.08.**

On the impingement surface, for the case of $\phi = 0^0$, the profiles of mean velocity (U) nondimensionalized with respect to the jet exit velocity ($U_0$) are plotted in Figure 5 versus the nondimensionalized normal distance (N) with respect to the jet exit width w, at 16 different r/w stations. $\phi = 0^0$ is in direction of the lateral coordinate (y-axis) The turbulence intensity profiles versus N/w at these stations are given in Figure 6. By using these profiles, the normalized maximum velocity of the r/w stations and half-velocity thickness, $N_{0.5}$, distribution are given in Figure 7. $N_{0.5}$ is normal to the impingement surface and shows the growth of the wall-bounded layer.

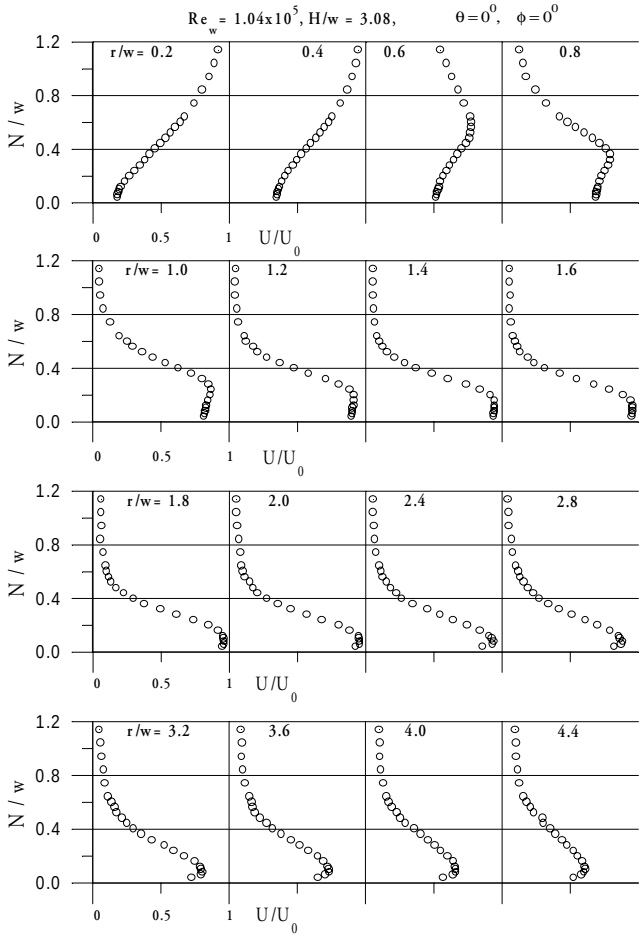


**Figure 5 Nondimensionalized velocity profiles versus $\phi = 0^0$ line at different r/w stations**

It can be seen from the Figures 5 and 7 that, the maximum mean velocity along $\phi = 0^0$ line, $U_M$, increases with increasing radial distance while the half velocity thickness, $N_{0.5}$, decreases. $U_M$ reaches a maximum value at r/w ≅ 1.8 measurement station as a value of $0.96U_0$ and after this point it decreases. $N_{0.5}$ reaches a minimum value at r/w ≅ 2.2 station as a value of 0.29w approximately and after this point it increases. The development of the $U_M/U_0$ and $N_{0.5}/w$ along the impingement surface are similar with the results of Landreth and Adrian [8] and Didden and Ho's [10] studies. After the r/w = 2.2 station, velocity profiles along normal distance shows a typical wall jet velocity distribution. A flat region exists at the velocity profile, in the region between N/w ≅ 0 and N/w ≅ 0.2 which is near the impingement surface for the r/w = 1.2 station. After this station the dimension of this flat region along normal distance N decreases with increasing radial distance and vanishes at r/w = 2.0, approximately.

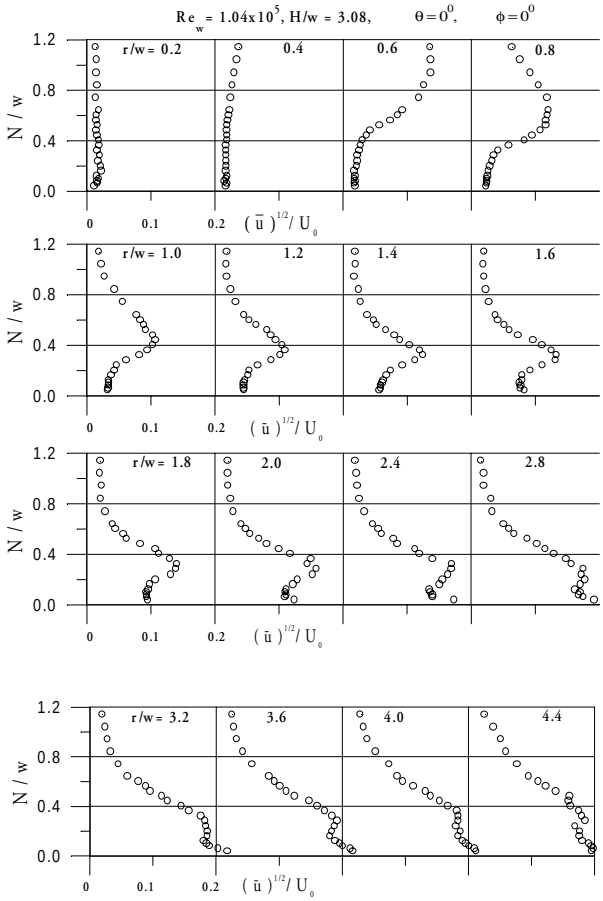


**Figure 6 Turbulence intensity profiles versus $\phi = 0^0$ at different r/w stations**

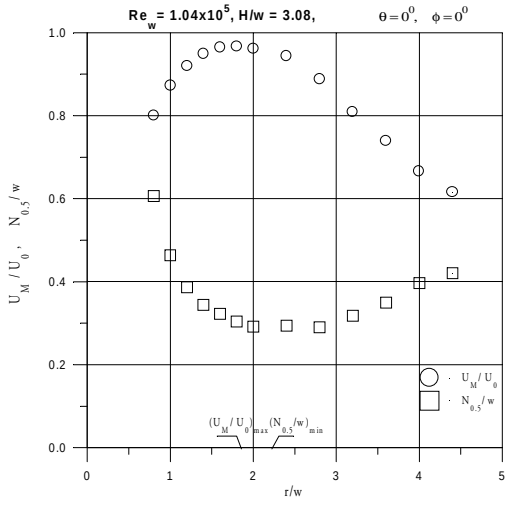


**Figure 7 The normalized maximum velocity and half-velocity thickness distribution along radial distance for $\phi = 0^0$ line.**

Near the stagnation point region, turbulence intensity profiles increase along normal distance and reach a maximum value where the inflexion point take place in the velocity profile. After this point turbulence intensity decreases as shown in Figure 6. After the r/w = 1.8 station, turbulence intensity profiles have two peaks near the impingement surface. Özdemir and Whitelaw [9] explain this structure that the mean velocity profile can cause large-scale disturbances with greater magnitude in the outer layer and small-scale disturbances close to the wall.

The development of the maximum velocity and half-velocity thickness along $\phi = 0^0$ and $\phi = 90^0$ lines can be compared in Figure 8. and indicated that because of the rectangular shape of the nozzle exit, for $\phi = 0^0$ line, $U_M$ and $N_{0.5}$ reach their maximum and minimum values at radial distances earlier than $\phi = 90^0$ line.

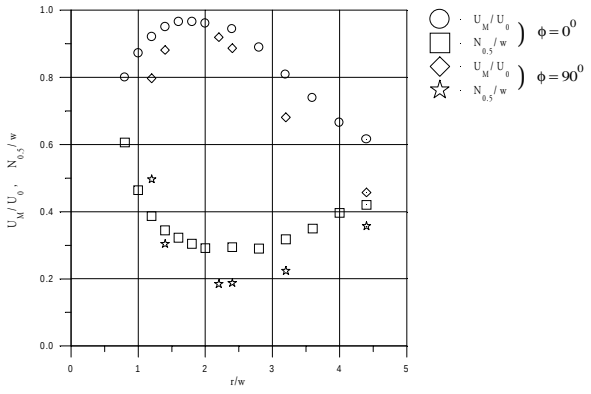


**Figure 8 The normalized maximum velocity and half-velocity thickness distribution along normalized radial distance.**

The impingement of a jet on a flat plate also causes a pressure distribution along the surface. The pressure coefficient is calculated with the equation

$$c_p = \frac{P_i - P_{at}}{(P_{\max} - P_{at})_{\theta=0}}$$

where ($P_i$) is the measured time-averaged pressure at the impingement surface, ($P_{at}$) is the time-averaged ambient pressure and $P_{max}$ is the maximum time-averaged pressure at the surface which is obtained at the stagnation point for the $\theta = 0$ case.

The pressure coefficient distributions on the impingement surface are given in Figure 9. $c_p$ value is "1" at the stagnation point, which is the center of axis system, and decreases to "0" at r/w ≅ 2.0 station rapidly. This rapid decrease in pressure coefficient indicates the equivalent rapid deflection of the jet streamlines and strong acceleration in the impingement flow to either side of the stagnation point [9]. Because of the rectangular shape of the nozzle exit geometry, $c_p$ decrease to "0" value more rapidly at $\phi = 0^0$ line comparing to $\phi = 90^0$ line.

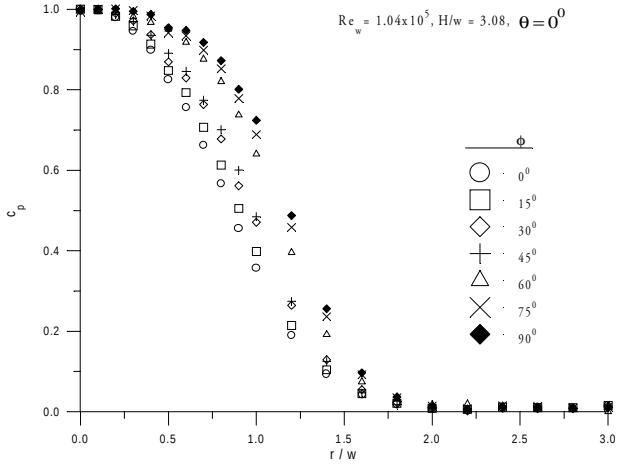


**Figure 9 Pressure coefficient distribution on the impingement surface.**

## 3.2 The Effect of the Impingement Angle on the Flow Structure of Jet Impingement.

To examine the effect of the θ angle between the jet centerline axis and the surface normal axis, this angle is taken as $0^0$, $5^0$, $10^0$, $15^0$ and $20^0$.

The photograph in the x-y plane of the impingement jet for the case of H/w = 3.08 and $\theta = 10^0$ is given in Figure 10 by using smoke flow visualization technique. Figure shows that, the inflowing coming flow is deflected in the $\phi = 0^0$ and $\phi = 180^0$ directions and there is two different flow type: near the stagnation point, at

$\phi = 180^0$ line which is left side of the figure, the flow dimension along normal distance is thicker according to $\phi = {}^0$ line. But after some distance from the stagnation point flow dimension at $\phi = 0^0$ line is thicker than $\phi = 180^0$ line.

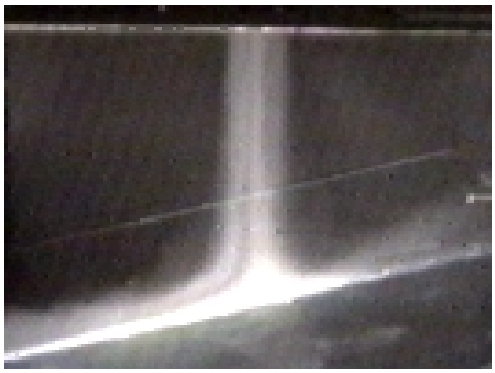

$\phi = 180^0$ $\phi = 0^0$

**Figure 10 The photograph of the impingement in the x-y free jet coordinate system plane for the case of H/w = 3.08 and $\theta = 10^0$**

The nondimensional velocity profiles on the impingement surface along $\phi = 180^0$ line are given in Figures 11 and 12 for $\theta = 0^0$ and $10^0$. Turbulence intensity profiles for these stations are given in Figures 13 and 14. For the same cases variations of the normalized maximum velocity and half-velocity thickness with radial distance are given in Figure 15.

As it can be seen from the Figures 11,12 and 15, the maximum mean velocity, $U_M$, decreases comparing to $\theta = 0^0$ case, but this decrement is higher at $\phi = 0^0$ line. Comparing to $\theta = 0^0$ case, half-velocity thickness, $N_{0.5}$, increases at $\phi = 180^0$ line which means faster growth and decreases at $\phi = 0^0$ line which means slower growth. The different behaviour of $N_{0.5}$ at $\phi = 0^0$ and $180^0$ lines indicates that there is a non-symmetric growth of the wall jet. The location of maximum velocity do not seem significantly influenced by $\theta$. The normalized maximum velocity and half-velocity thickness change linearly with radial distance after the r/w $\cong$ 2.2. Similar results are given by Araujo et al [7].

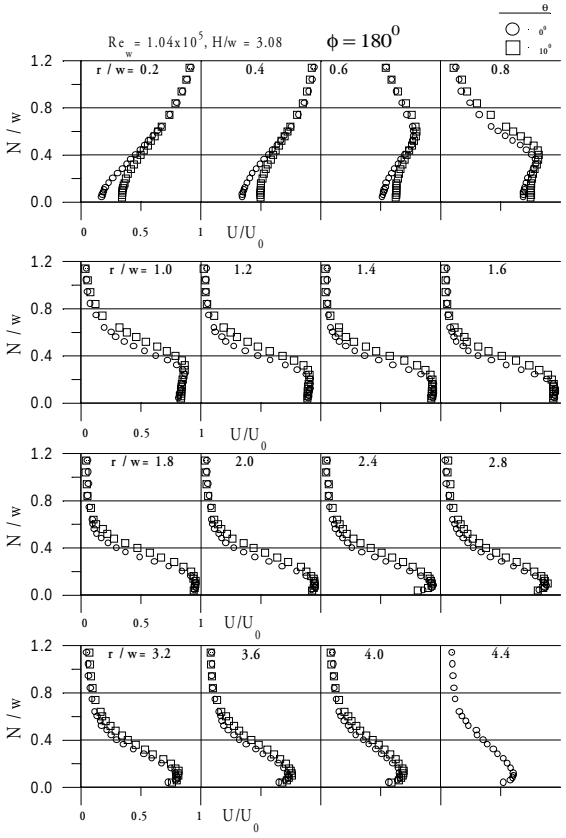


**Figure 11 Nondimensionalized velocity profiles versus N/w at r/w stations of $\phi = 180^0$ line for different $\theta$ values.**

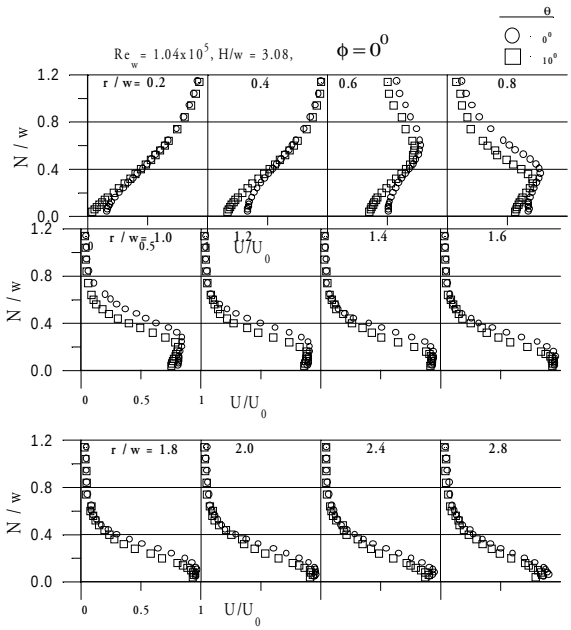


**Figure 12 Nondimensionalized velocity profiles versus N/w at r/w stations of $\phi = 0^0$ line for different $\theta$ values.**

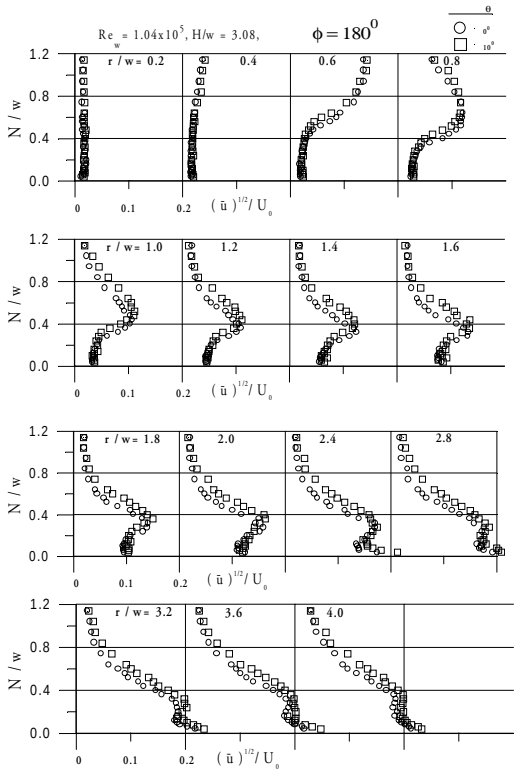


**Figure 13 Turbulence intensity profiles versus N/w at r/w stations of $\phi = 180^0$ line for different θ values.**

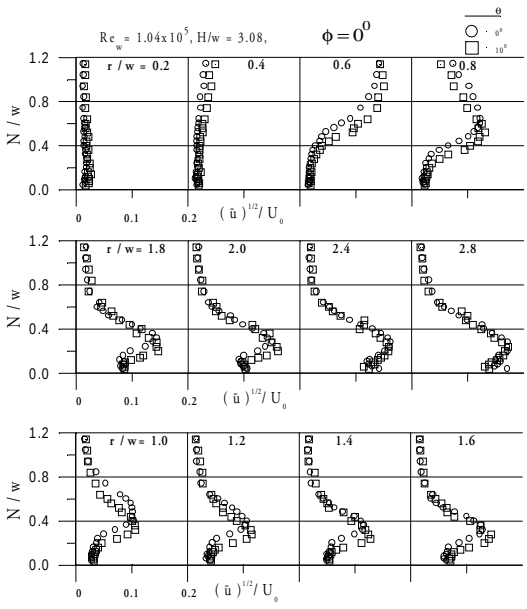


**Figure 14 Turbulence intensity profiles versus N/w at r/w stations of $\phi = 0^0$ line for different θ values.**

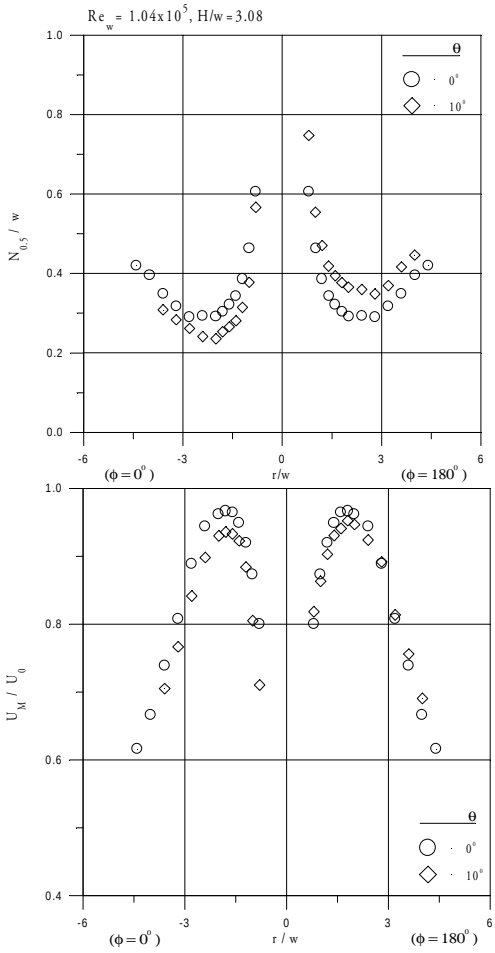


**Figure 15 The normalized maximum velocity and half-velocity thickness distribution along normalized radial distance for $\theta = 0^0$ and $10^0$, H/w = 3.08.**

Figures 13 and 14 shows that, giving an increment to θ as $10^0$ does not affect distinctly the shape of the turbulence intensity profiles. For $\phi = 180^0$ line, after r/w ≅ 2.0 station, turbulence intensity along normal distance at r/w stations increases with θ. Turbulence intensity along normal distance at $\phi = 0^0$ line increases with increasing θ values in the region near to the surface, between $0.6 \le r/w \le 2.0$.

The pressure coefficient distributions on the impingement surface along $\phi = 0^0$ and $\phi = 180^0$ lines are given in Figures 16 and 17 for $\theta = 0^0$ and $10^0$. These figures show that the stagnation point moves backward along the line of incidence. As a consequence the value of the pressure coefficient at the centre of the axis system decrease with increasing value of θ.

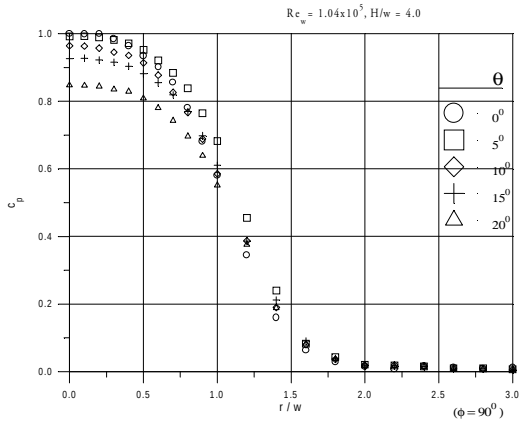


**Figure 16 Pressure coefficient distribution on the impingement surface along radial distance for different θ values.**

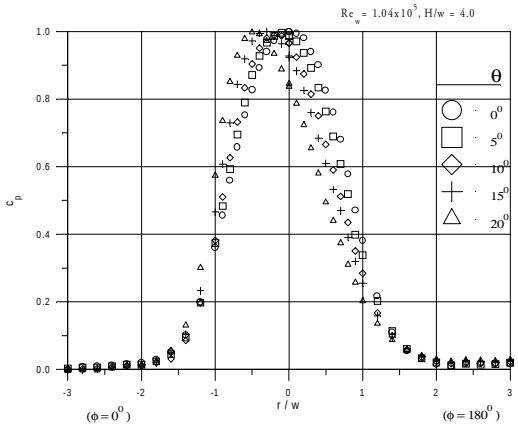


**Figure 17 Pressure coefficient distribution on the impingement surface along $\phi = 90^0$.**

Figures 13,15,16 and 17 indicate that the flow on the impingement surface has a wall jet character after a r/w distance at which the pressure coefficient vanishes. The flat region of the velocity profile appears first at the r/w station on which $c_p \cong 0.6$ for $\phi = 180^0$ and $c_p \cong 0.4$ for $\phi = 0^0$. Flat region disappears at the point $c_p$ vanishes.

Özdemir and Whitelaw [9] uses the maximum value of the mean velocity, $U_M$, as the scaling parameter for the velocity of the wall flow at each measuring position and uses the half-velocity thickness, $N_{0.5}$, for the normalization of the normal distance. $N_{0.5}$ represents the growth of the inner wall bounded and outer free shear layers. By using these scaling parameters, the normalized profiles of mean velocity $U / U_M$ at different r/w stations on $\phi = 180^0$ line are given in Figures 18 for $\theta = 0^0$ and $10^0$.

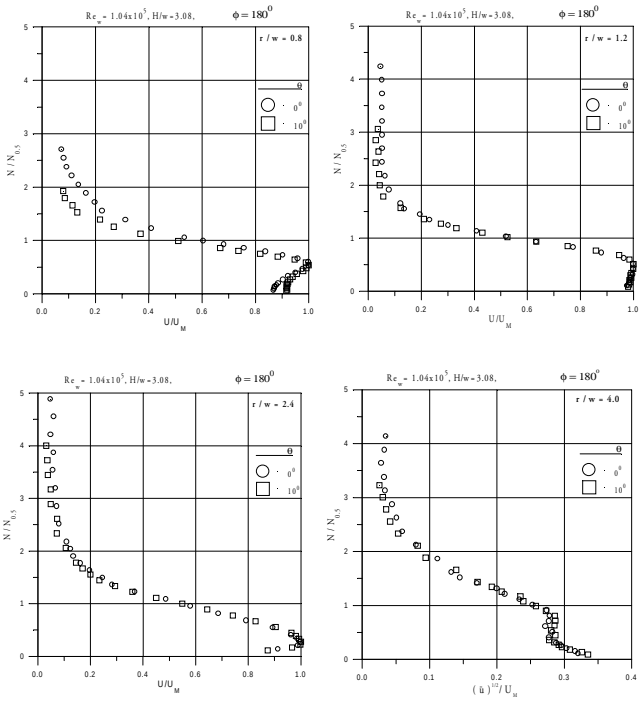


**Figure 18 Profiles of normalized velocity by using the scaling parameters $U_M$ and $N_{0.5}$ , along normal distance for $\theta = 0^0$ and $10^0$, $\phi = 180^0$.**

Figure 18 indicates that, for $\phi = 180^0$ line, at each station after r/w ≅ 1.2 the velocity profiles for $\theta = 0^0$ and $10^0$ are nearly coincide. Araujo et al [7] found the similar result indicating the non-dimensional velocity distributions are independent of the small vales of θ.

## 4 Conclusions

The objective of this study is to investigate experimentally the rectangular (h/w = 2) jet flow that impinges to a flat plate normally and obliquely. Reynolds numbers based on the nozzle exit width is $1.05x10^5$. To examine the effect of the angle between the jet centerline axis and the surface normal axis on the jet impingement characteristics, θ is taken as $0^0$, $5^0$, $10^0$, $15^0$ and $20^0$.

In front of the impingement surface, centerline velocity begins to decrease rapidly comparing to free jet condition. Near the impingement surface., velocity profiles become wider comparing to free jet case and begins to show "saddle-back" shape. Turbulence intensity profiles along y-axis become thicker but the maximum value of the turbulence intensity decreases.

There is stagnation point at the intersection point of the jet centerline with the surface. Surface streak lines show an elliptical growth although nozzle has a rectangular exit.

On the impingement surface, a flat region exists at the velocity profiles along normal distance N for $\phi = 0^0$ line which corresponds to the point where the pressure coefficient $c_p$ reaches to “0” value. After this station velocity profiles along N shows a typical wall jet velocity distribution.

The angle between the jet centerline axis and the surface normal axis, $\theta$, affects the flow structure of the jet impingement. Comparing to $\theta = 0^0$ case, half-velocity thickness, $N_{0.5}$, increases at $\phi = 180^0$ line which means faster growth and decreases at $\phi = 0^0$ line which means slower growth.

Giving an increment to $\theta$ as $10^0$ does not affect distinctly the shape of the turbulence intensity profiles along normal distance close to the surface at measurement stations of $\phi = 180^0$ line but turbulence intensity increases with $\theta$.

The pressure coefficient $c_p$ at the centre of the axis system decreases with increasing $\theta$ values, because stagnation point moves through $\phi = 0^0$ direction where the jet is coming with an angle from this side.

By using the scaling parameters as $U_M$ and $N_{0.5}$, the profiles of mean velocity and turbulence intensity along normal distance show similarity for $\theta = 0^0$ and $10^0$ cases after the r/w = 1.2 station for $\phi = 180^0$ line.

## References


[1] Marsters, G.F., "Spanwise Velocity Distributions on Jets from Rectangular Slots," *AIAA Journal*, Vol.19, No.2, pp.148, (1981).

[2] Quinn, W.R., "Passive Near-Field Mixing Enhancement in Rectangular Jet Flows," *AIAA Journal*, Vol.29, No.4, pp.515, (1991).

[3] Trentacoste, N., and Sforza, P.M., "Some Remarks on Three-Dimensional Wakes and Jets," *AIAA Journal*, Technical Note, Vol.6, No.12, pp.2454, (1968).

[4] Quinn, W.R., "Turbulent Mixing in a Free Jet Issuing from a Low Aspect Ratio Contoured Rectangular Nozzle," *The Aeronautical Jou*rnal, pp.337, (1995).

[5] Krothapalli, A., Baganoff, D., and Karamcheti, K., "On the Mixing of a Rectangular Jet," *Journal of Fluid Mechanics*, Vol.107, pp.201, (1981).

[6] Page, P.H., Hadden, L.L., and Ostowari, C., "Theory for Radial Jet Reattachment Flow," *AIAA Journal*, Vol.27, No.11, pp.1500, (1989).

[7] Araujo, S.R.B., Durao, D.F.G., and Firmino, F.J.C., "Jets Impinging Normally and Obliquely to a Wall," *AGARD*, CP-308, (1981).

[8] Landreth, C.C., and Adrian, R.J., "Impingement of a Low Reynolds Number Turbulent Circular Jet onto a Flat Plate at Normal Incidence," *Experiments in Fluids*, Vol.9, pp.74, (1990).

[9] Özdemir, I.B., and Whitelaw, J.H., "Impingement of an Axisymmetric Jet on Unheated and Heated Flat Plates," *Journal of Fluid Mechanics*, Vol.240, pp.503, (1992).

[10] Didden, N., and Ho, C-M, "Unsteady Seperation in a Boundary Layer Produced by an Impinging Jet," *Journal of Fluid Mechanics*, Vol.160, pp.235, (1985).